Supporting Information

Side Chain Engineering of Indacenodithieno[3,2-*b*]thiophene (IDTT)-Based Wide Bandgap Polymers for Non-Fullerene Organic Photovoltaic

Zehua He[1,2†], Tingting Dai[2†], Ting Meng[2], Peng Lei[2], Yanfang Geng[2], Linjiao Qin[1,2], Jiang Wu[1,2], Jiagui Yu[1,2], Qingdao Zeng[2], Erjun Zhou*[2]*

[1] Henan Institutes of Advanced Technology, Zhengzhou University, Zhengzhou 450003, China.
[2] CAS Center for Excellence in Nanoscience, National Center for Nanoscience and Technology, Beijing 100190, China.
E-mail: gengyf@nanoctr.cn, zhouej@nanoctr.cn

[†] These authors contributed equally to this work.

Measurements and characterizations

^{1}H NMR (400 MHz) and ^{13}C NMR (100 MHz) were measured with a Bruker AVANCE 400 spectrometer in deuterated trichloromethane ($CDCl_3$). Chemical shifts are given in ppm units using tetramethylsilane (TMS) as an internal standard. Mass spectra were collected on an Autoflex MAX mass spectrometer. Molecular weights of the polymers were measured on Angilent Technologies PL-GPC 220 high-temperature-chromatograph at 150 °C using a calibration curve of polystyrene standards and 1,2,4-trichlorobenzene as the eluent. Thermo-gravimetric analysis (TGA) was measured by Diamond TG/DTA under the protection of nitrogen at a heating rate of 10 °C /minute. UV–vis absorption spectra were obtained by Lambda-950 (Perkin Elmer Instruments Co. Ltd., America). The solution samples were prepared using CF solvent with a concentration of 0.01mg/ml. And temperature-dependent UV absorption spectra were prepared using CB solvent, the absorption spectrum was measured for each 20°C increase in temperature (from 30°C to 110°C). The molecular energy levels were measured by utilizing CHL600E Electrochemical Workstation via cyclic voltammetry methods. The Pt plate coated with a thin film was employed as working electrode, an Ag/AgCl reference electrode and a Pt wire counter electrode were also employed as the another two of the three electrodes. The measurements were carried out in anhydrous acetonitrile with tetrabutylammonium hexafluorophosphate (0.1mol L^{-1}) under the argon atmosphere at a scan rate of 100mV/s. The ferrocene/ferrocenium redox couple (Fc/Fc^{+}) was employed to calibrate the potential of Ag/AgCl reference electrode. The $J-V$ curves were measured in air with a Keithley 2420 source measure unit. An Oriel Newport 150W solar simulator was used to carry out the AM 1.5G irradiation condition and the light intensity was calibrated with a Newport reference detector (Oriel PN 91150V). An Oriel Newport system (Model 66902) was applied for the external quantum efficiency (EQE) measurements of the devices in air. The mobility of electron-only and hole-only devices were tested by a Newport Thermal Oriel 91159A. Highly sensitive EQE was measured by using an integrated system (PECT-600, Enlitech), in which the photocurrent was amplified and modulated by a lock-in instrument. EQE_{EL}

values were obtained by applying external voltage/current sources through the devices (ELCT-3010, Enlitech). EQE_{EL} measurements were performed for all devices according to the optimal device preparation conditions. TRPL was recorded by TCSPC (Becker & Hickl, SPC-150).Two-dimensional grazing incidence wide angle X-ray scattering (2D-GIWAX) analyses were measured at the XEUSS SAXS/WAXS equipment. The data were obtained with an area Pilatus 100k detector with a resolution of 195 × 487 pixels (0.172 mm × 0.172 mm). The X-ray wavelength was 154 nm, and the incidence angle was 0.2°. The samples were spin-coated onto the PEDOT: PSS/Si substrate with the optimized device fabrication conditions. AFM images were obtained on a Multimode 8 HR in the intelligent mode.

OPV device fabrication and characterization of photovoltaic cells

The cleaned glass substrates with ITO electrode were used, the ITO glass substrates were blown by nitrogen gas and was put into an ultraviolet ozone chamber for 15 minutes before using. Then the PEDOT: PSS was spin-coated onto the ITO glass (3000 r/min) and heated at 150°C for 15 min. The optimal Donor: Acceptor (D: A) ratio was 1:1.5 (w/w) for all polymers, were dissolved in chloroform (CF) with a total concentration of 15 mg/mL for 1 hour at 50°C and then the active layers were spin-coated onto the substrates with specific speed (**Table S1-S3**) at a glove box filled with nitrogen. The PDINO was spin-coated onto the ITO glasses with a speed 3000 r/min. Finally, negative electrode aluminum was evaporated onto the surface of the active layer.

Carrier mobility characterization

The carrier mobilities of the polymers were estimated by the space charge limited current (SCLC) method. The hole only devices were fabricated with the order ITO/PEDOT: PSS/active layer/Au and the electron mobility of the blends were with the structure of ITO/TiOx/active layer/PDINO/Al. The SCLC model can be operated followed Mott-Gurney law, as the equation $J=(9/8)\varepsilon_0\varepsilon_r\mu (V^2/L^3)$, J is the current

density, ε_0 is the permittivity of free space, ε_r is the relative dielectric constant of the transport medium, μ is the carrier mobility, V is the internal potential in the device and L is the film thickness of the active layer. For example: The thickness of three active layer based on **PIDTT-Th**: Y6/**PIDTT-Ph**: Y6/**PIDTT-PhF**: Y6 are estimated to be 101.73, 107.55, and 90.83nm for the electron-only devices and 100.26, 104.30 and 119.35 nm for the hole-only devices, respectively.

Quantum chemical calculations:

The quantum chemical calculations were performed using density functional theory (DFT) B3LYP functional with the 6-31G (*d*, *p*) basis set. Alkyl chains were replaced by methyl groups to simplify the structures and reduce the calculation costs.

Materials and Synthesis

Materials

All chemicals and solvents were reagent grades, which were purchased from Alfa, ACMEC, Bidepharm, TCI, J&K Scientific, Beijing Chemical Plant or other chemical companies. Chemicals and solvents were used without further purification (unless otherwise noted). Monomer **1** was purchased from above companies and monomer **2**, monomer **3** were synthesized according to the reported procedures.[1, 2]

Synthesis of monomer 3

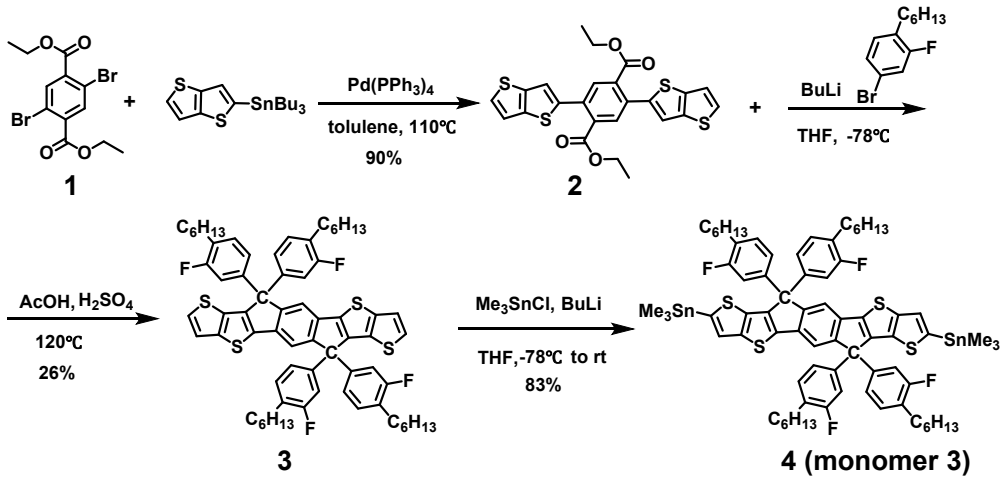

Scheme S1. Synthetic route of monomer **3** (compound 4)

Synthesis of diethyl 2,5-bis(thieno[3,2-b]thiophen-2-yl)terephthalate compound 2: Diethyl-2,5-dibromoterephthalate (**1**) (380 mg, 1.0 mmol), tributyl(thieno[3,2-b]thiophen -2-yl)stannane (944.39 mg, 2.2 mmol) and catalyst were added to a 50 mL Schlenk flask and then 18 mL toluene was dropped into the flask. The reaction flask was vacuumed, then filled with nitrogen and repeated several times. The reaction flask was then stirred at 110 ℃ for 24 hours. After the reaction, the solution was cooled to room temperature, the organic phase was extracted with dichloromethane, and the excess solvent was removed by spin evaporation. Crude product was purified by column chromatography using DCM/PE (1:5) as the eluent. Orange solid was obtained with a yield of 90% (0.45 g). ^{1}H NMR (400 MHz, Chloroform-*d*): δ 7.92 (s, 2H), 7.43 (d, *J* = 5.3 Hz, 2H), 7.35 – 7.29 (m, 4H), 4.27 (q, *J* = 7.1 Hz, 4H), 1.16 (t, *J* = 7.1 Hz, 6H); ^{13}C NMR (101 MHz, $CDCl_3$): δ 13.84, 61.83, 76.72, 77.04, 77.36, 119.31, 119.43, 127.40, 132.09, 133.81, 134.10, 139.39, 139.94, 142.03, 167.46; MALDI-TOF MS: calcd for $C_{24}H_{18}O_4S_4$, 498.0 (m/z); found, 498.1(M+).

Synthesis of compound 3:

Compound **2** (997.29 mg, 2.0 mmol) was dissolved into 15 mL THF. The solvent was cooled to -78°C and n-butyllithium was added under nitrogen protection. After 1 h stirring, 4-bromo-2-fluoro-1-hexylbenzene (2.30 g, 9.6 mol) was added into the flask. Then the solvent was warmed naturally to room temperature and reacted overnight. The crude product was extracted with ethyl acetate and proceeded directly to the next step reaction.

The crude product was dissolved into 50 mL acetic acid and then 2.88 mL concentrated sulfuric acid was slowly dropped into the solution. The reaction was stirred 2 h at 120℃, then cooled to room temperature. After extracted with n-hexane and dichloromethane, the excess solvent was removed by spin evaporation. Then the crude product was purified by column chromatography using DCM/PE (1:10) as the eluent. Orange solid was obtained with a yield of 26% (0.57g). ^{1}H NMR (400 MHz, Chloroform-*d*): δ 7.50 (s, 2H), 7.33 (s, 4H), 7.12 (t, *J* = 8.0 Hz, 4H), 7.04 – 6.90 (m, 8H), 2.60 (t, *J* = 7.8 Hz, 8H), 1.66 – 1.56 (m, 9H), 1.43 – 1.33 (m, 11H), 1.33 – 1.25

(m, 14H), 0.90 (q, *J* = 7.1 Hz, 13H); ^{13}C NMR (101 MHz, $CDCl_3$) δ 0.02, 14.08, 22.58, 28.78, 29.17, 30.00, 31.63, 62.53, 76.71, 77.03, 77.35, 114.88, 115.11, 116.91, 120.49, 123.56, 123.59, 123.85, 126.82, 128.70, 128.86, 130.59, 130.65, 133.35, 133.44, 136.19, 141.99, 142.03, 142.06, 143.33, 143.38, 143.46, 145.04, 152.40, 152.55, 152.63, 159.80, 162.23; MALDI-TOF MS: calcd for $C_{68}H_{70}F_4S_4$, 1090.4 (m/z); found, 1090.5 (M+).

Synthesis of compound 4:

Compound **4** (218.31 mg, 0.2 mmol) was dissolved into 15 mL THF. The solvent was cooled to -78℃ and n-butyllithium was added under the nitrogen protection. After stirring for 1 h, $(CH_3)_3SnCl$ (119.56 mg, 0.6 mmol) was added and then the mixture was stirred overnight. The crude product was extracted with chloroform, and purified by recrystallization, yield yellow solid was obtained with a yield of 83% (0.20 g). ^{1}H NMR (400 MHz, Chloroform-*d*): δ 7.46 (s, 2H), 7.35 (s, 2H), 7.12 (t, *J* = 8.0 Hz, 4H), 7.05 – 6.90 (m, 8H), 2.60 (t, *J* = 7.8 Hz, 8H), 1.65 – 1.56 (m, 10H), 1.41 (s, 1H), 1.39 – 1.31 (m, 18H), 1.30 (d, *J* = 4.3 Hz, 5H), 0.90 (q, *J* = 6.9 Hz, 13H), 0.42 (s, 18H); ^{13}C NMR (101 MHz, $CDCl_3$): δ -8.07, 13.93, 14.09, 22.23, 22.59, 28.78, 28.80, 29.17, 29.19, 29.99, 31.41, 31.64, 62.50, 76.71, 77.03, 77.34, 114.91, 115.15, 116.86, 123.65, 123.68, 127.52, 128.52, 128.68, 130.52, 130.58, 136.33, 138.96, 141.06, 142.22, 142.29, 143.32, 144.13, 144.51, 152.40, 159.77, 162.20; MALDI-TOF MS: calcd for $C_{74}H_{86}F_4S_4Sn_2$, 1416.4 (m/z); found, 1416.3 (M+).

Synthesis of PIDTT-Th

Monomer **1** (201.78 mg, 0.15 mmol) , 4,7-bis(5-bromo-6-hexylthieno[3,2-b] thiophen-2-yl)-5, 6-difluoro-2-(2-hexyldecyl)-2H-benzo[d][1,2,3]triazole (147.30 mg, 0.15 mmol) and catalyst dissolved into 12 mL ultra-dry toluene. And then the reaction was stirred at 110 ℃ for 48 h. Red solid **PIDTT-Ph** was obtained with a yield of 90% (252.17 mg).

Synthesis of PIDTT-Ph

Monomer **2** (205.53 mg, 0.15 mmol), 4,7-bis(5-bromo-6-hexylthieno[3,2-b] thiophen-2-yl)-5, 6-difluoro-2-(2-hexyldecyl)-2H-benzo[d][1,2,3]triazole (147.30 mg, 0.15 mmol) and catalyst dissolved into 12 mL ultra-dry toluene. After stirring at 110 ℃ for 48 h, red solid **PIDTT-Th** was obtained with a yield of 91% (255.38 mg).

Synthesis of PIDTT-PhF

Compound **3** (212.55 mg, 0.15 mmol), 4,7-bis(5-bromo-6-hexylthieno[3,2-b]thiophen-2-yl)-5,6-difluoro-2-(2-hexyldecyl)-2H-benzo[d][1,2,3]triazole (147.30 mg, 0.15 mmol) and catalyst were dissolved into 12 mL ultra-dry toluene. And then the reaction was stirred at 110℃ for 48 h. 265.06 mg red solid was obtained with a yield of 91%.

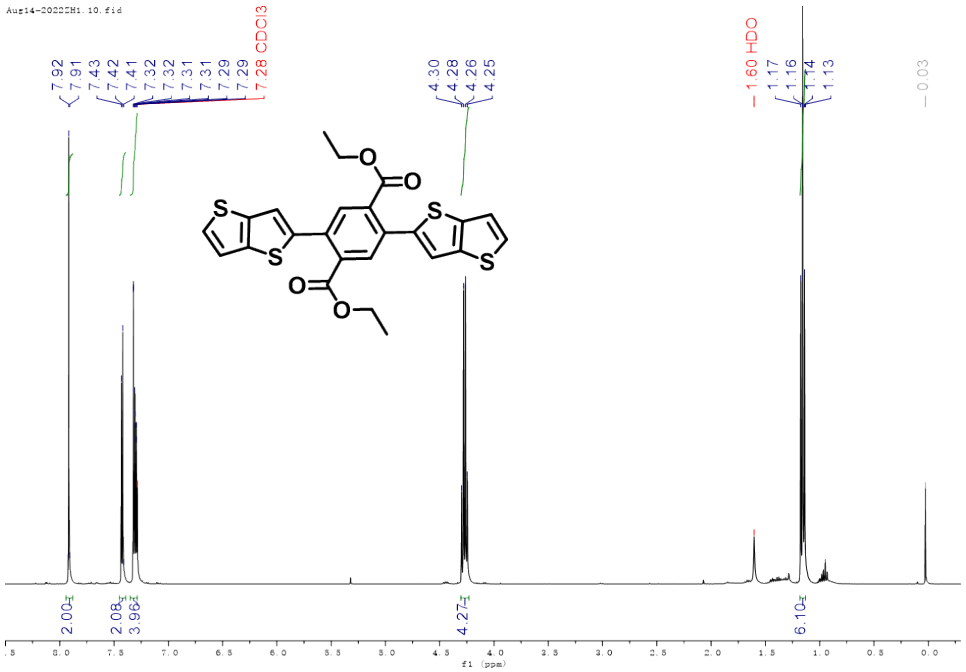

Figure S1. ^{1}H NMR spectrum of compound **2** at room temperature (400 MHz, Chloroform-*d*).

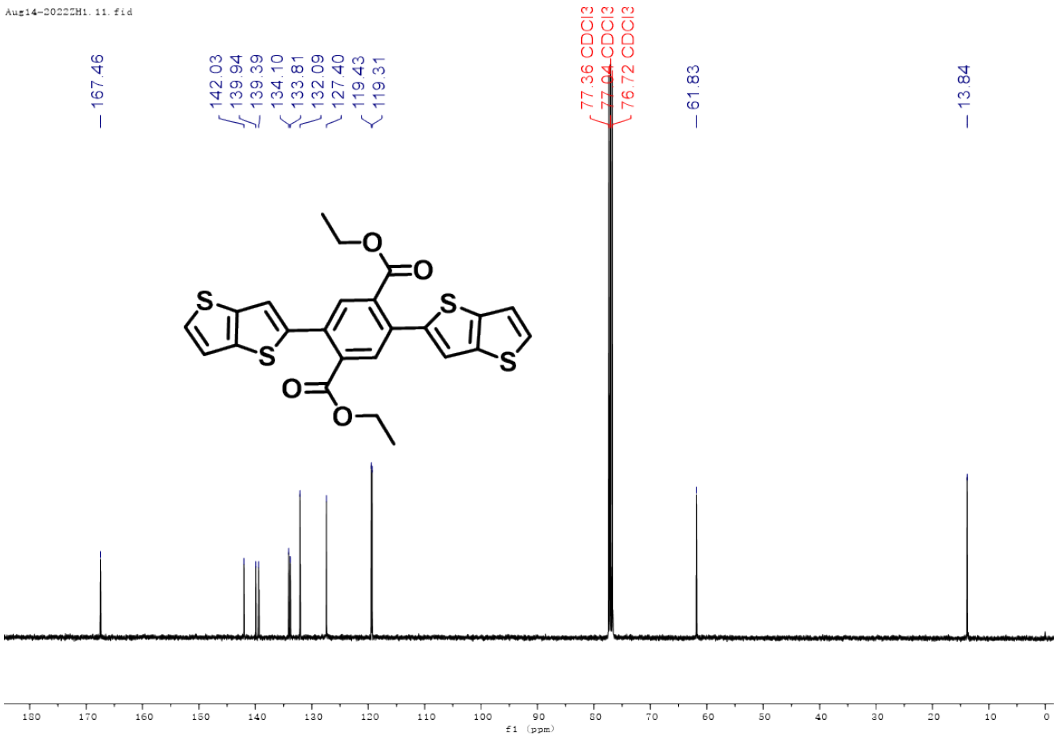

Figure S2. ^{13}C NMR spectrum of compound **2** at room temperature (101 MHz, $CDCl_3$)

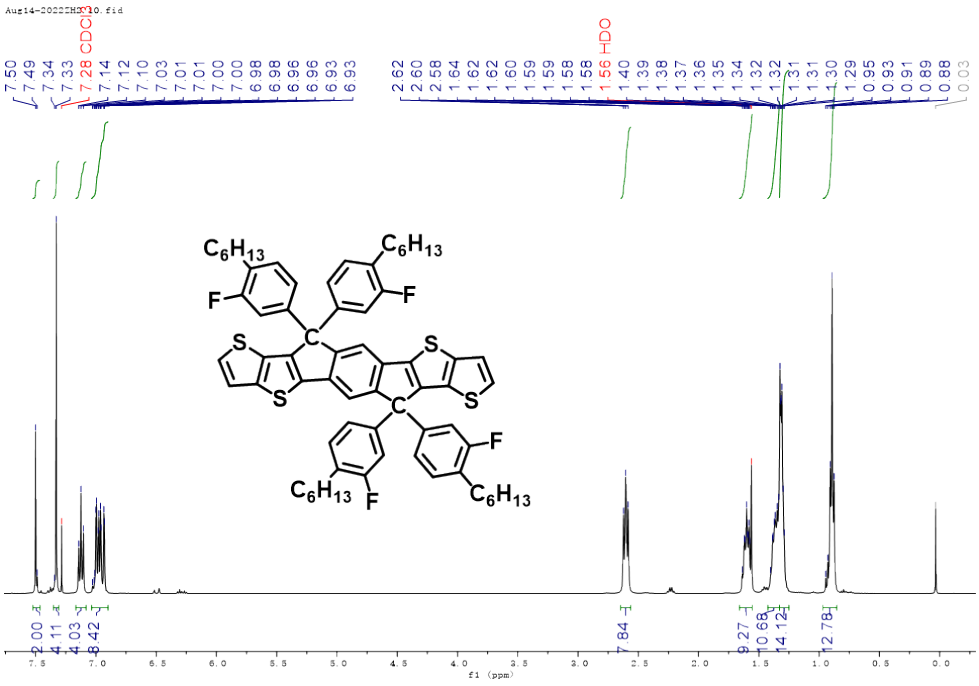

Figure S3. ^{1}H NMR spectrum of compound **3** at room temperature (400 MHz, Chloroform-*d*).

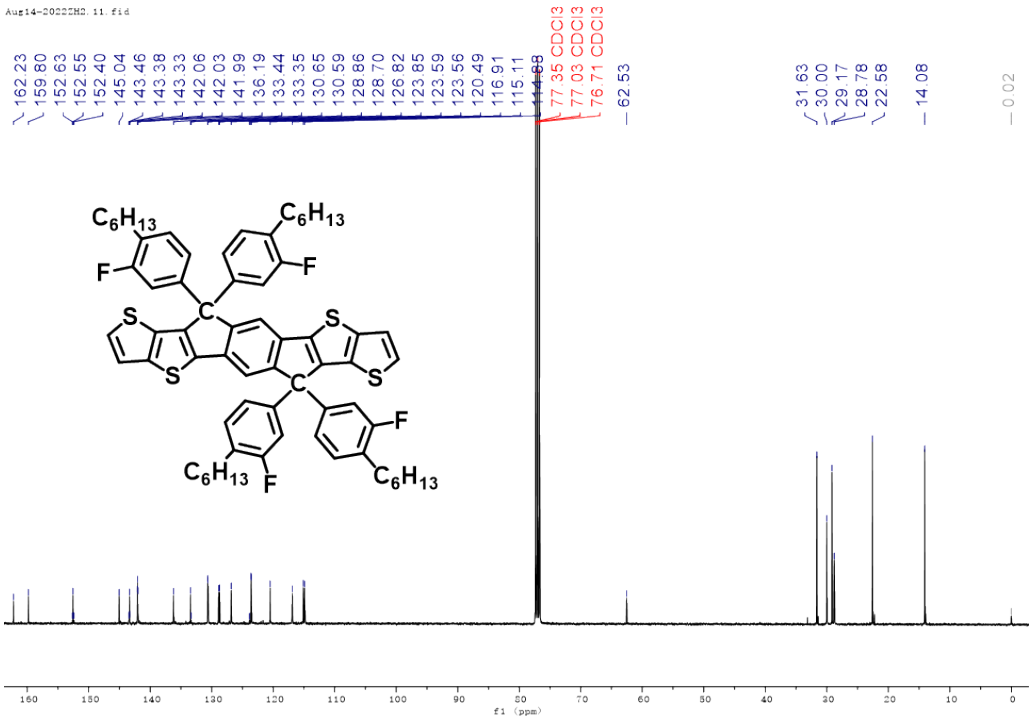

Figure S4. ^{13}C NMR spectrum of compound **3** at room temperature (101 MHz, $CDCl_3$)

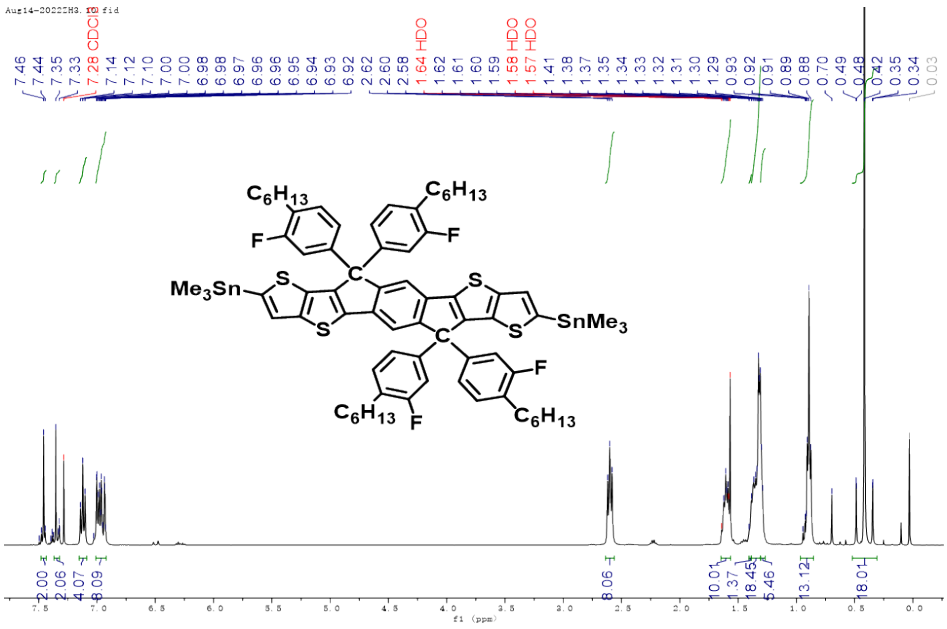

Figure S5. ^{1}H NMR spectrum of compound **4** at room temperature (400 MHz, Chloroform-*d*).

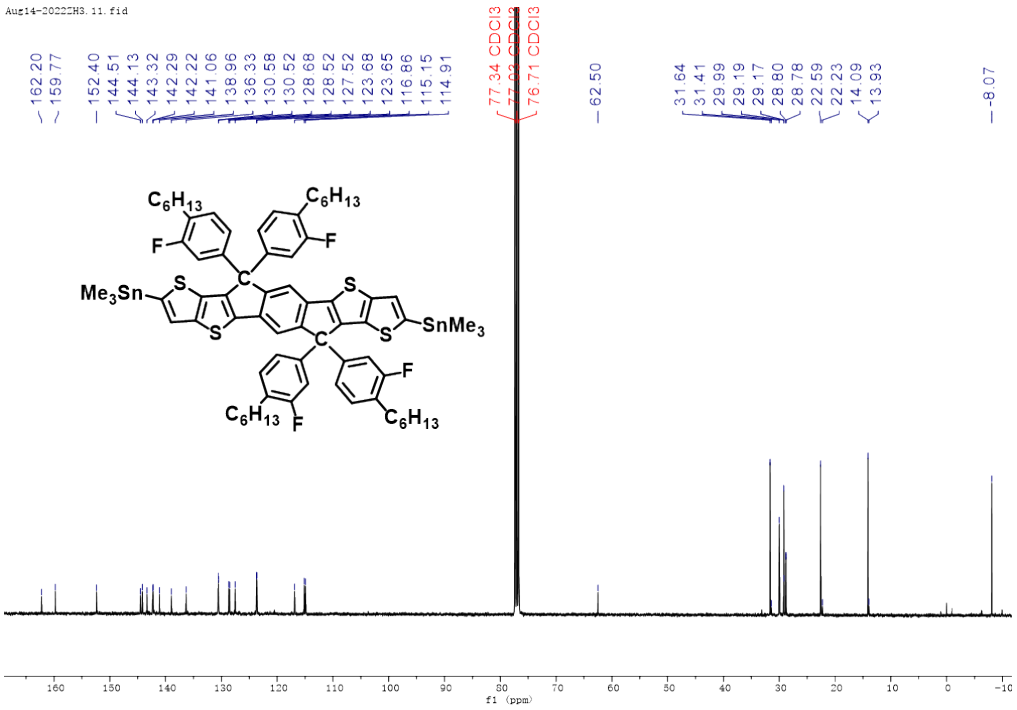

Figure S6. ^{13}C NMR spectrum of compound **4** at room temperature (101 MHz, $CDCl_3$)

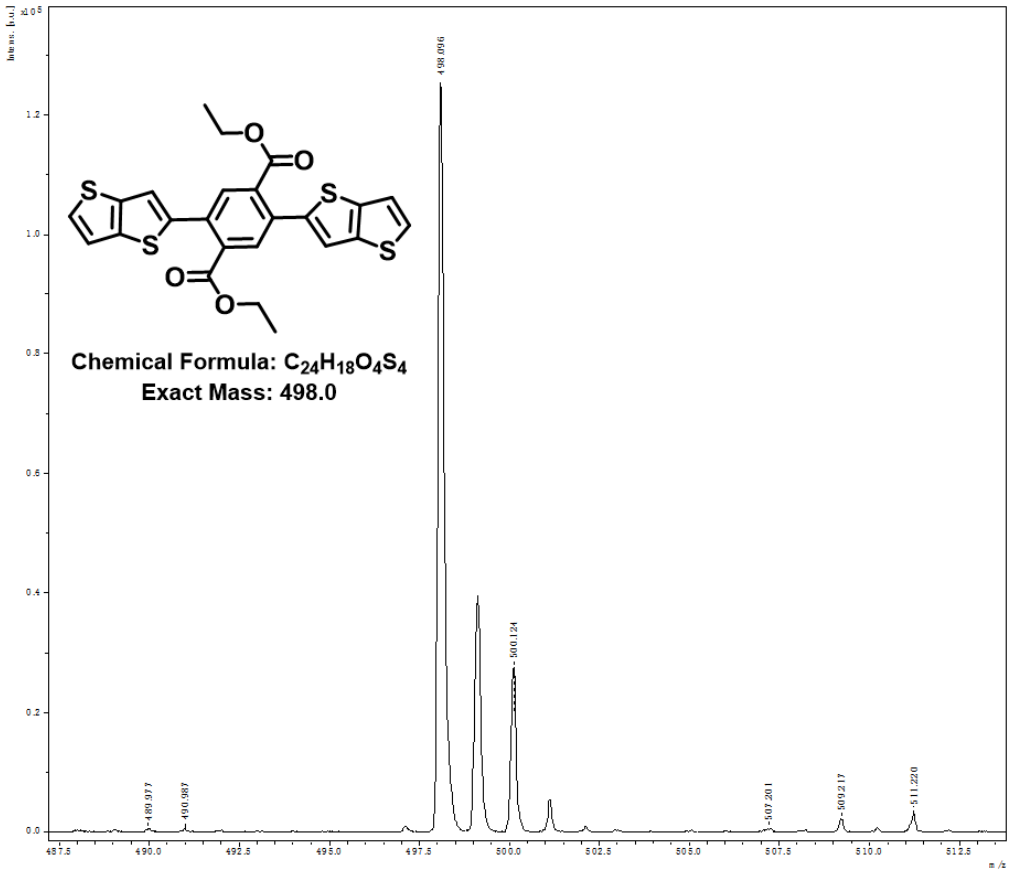

Figure S7. MS spectrum (MALDI-TOF) of compound **2**.

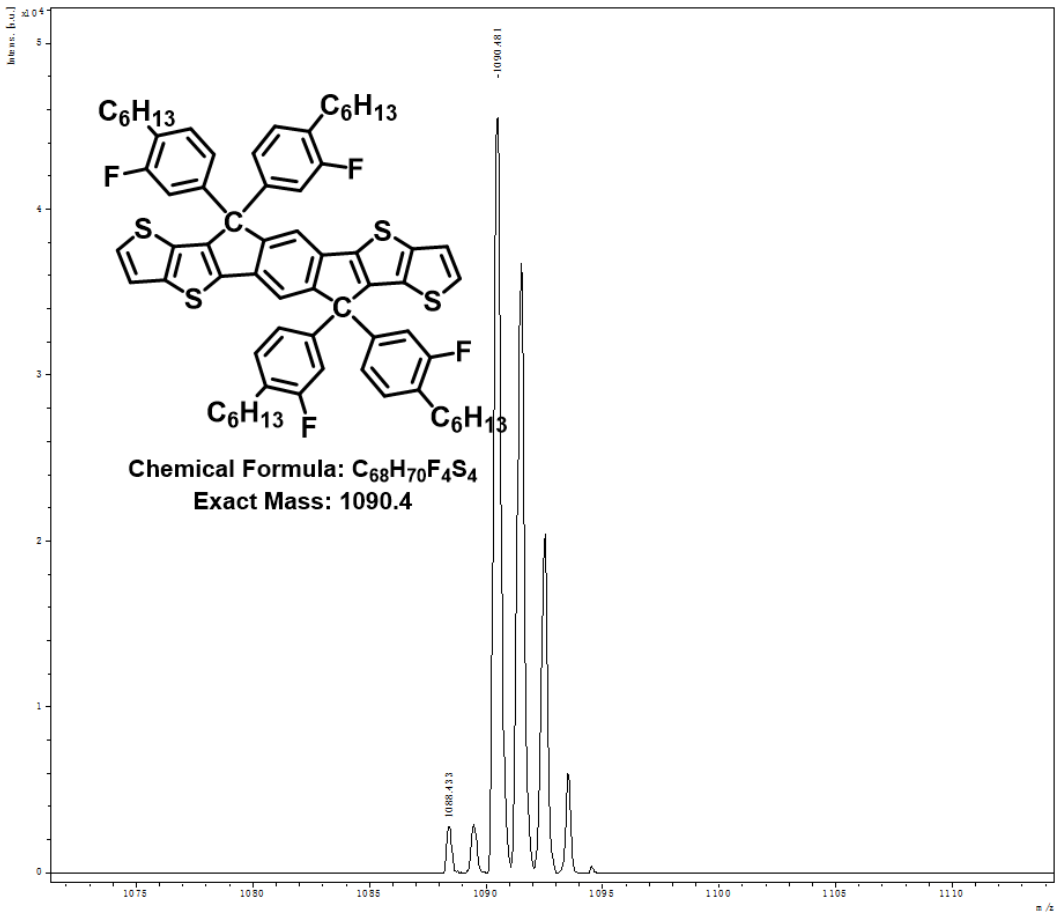

Figure S8. MS spectrum (MALDI-TOF) of compound **3**.

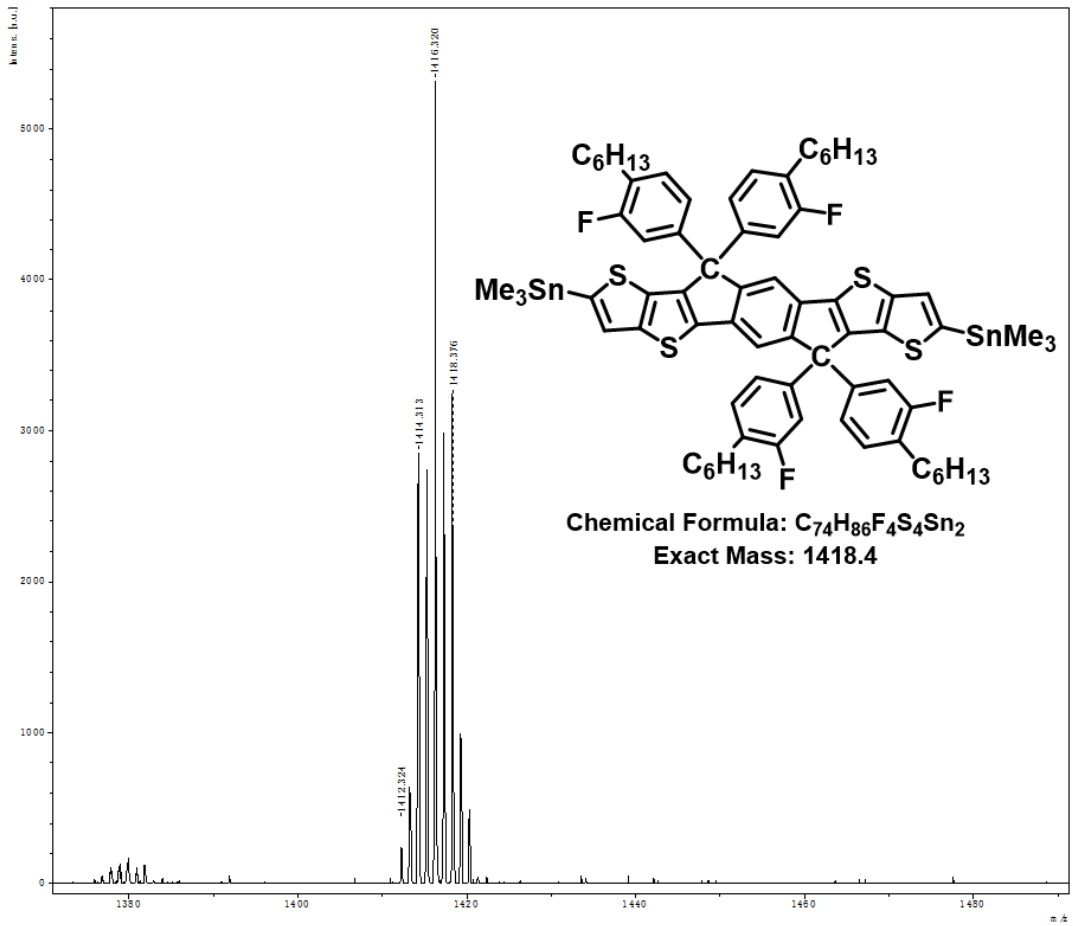

Figure S9. MS spectrum (MALDI-TOF) of compound **4**.

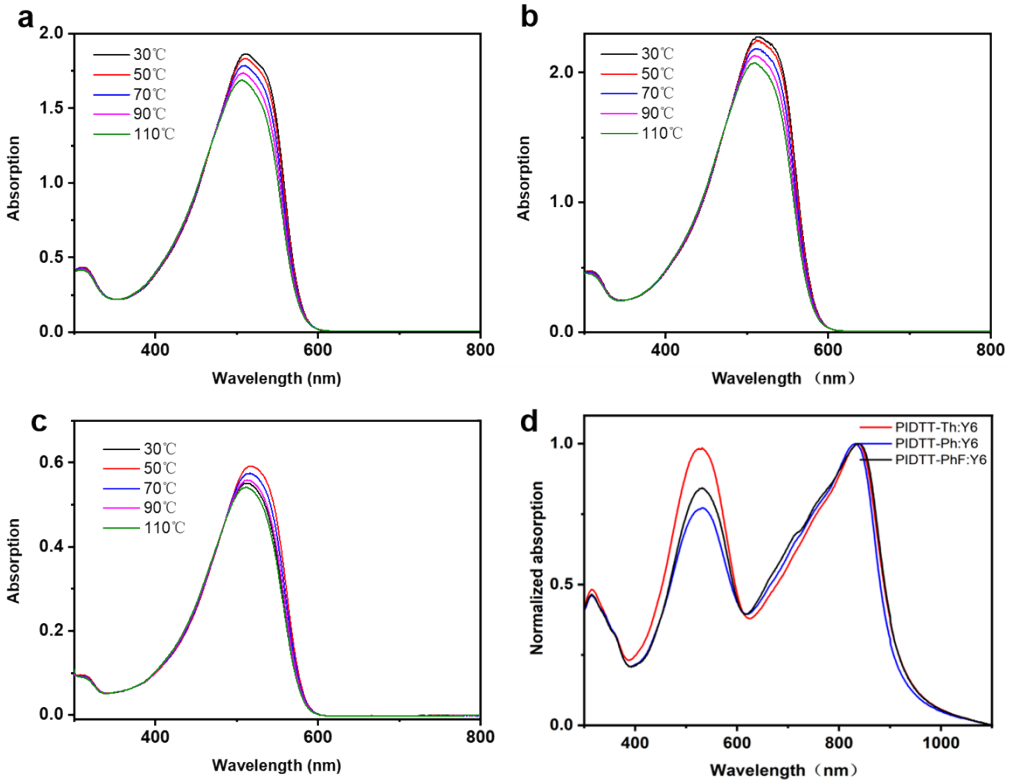

Figure S10. Temperature-dependent UV absorption spectra of (a) PIDTT-Th, (b) PIDTT-Ph, (c) PIDTT-PhF and (d) normalized absorption of blend films.

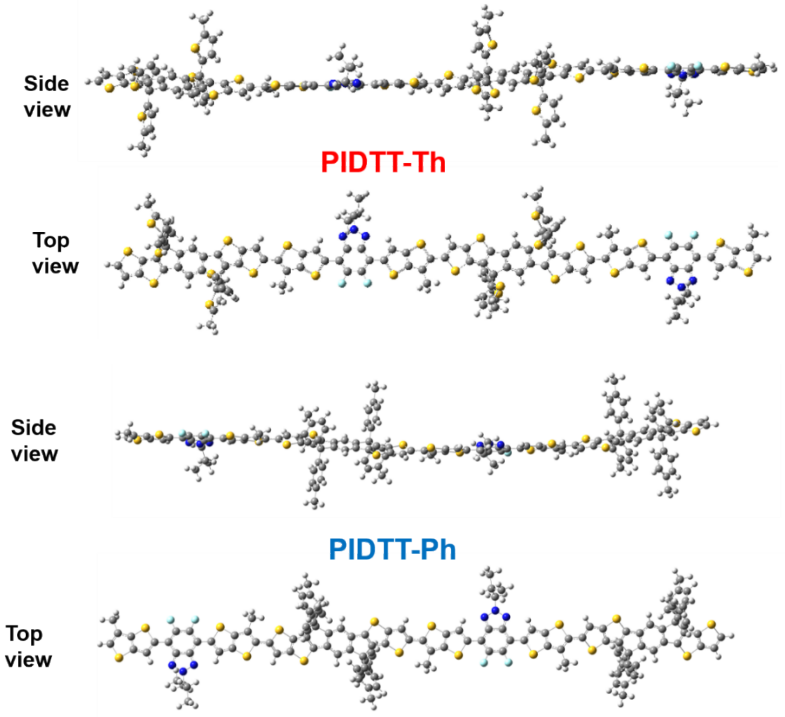

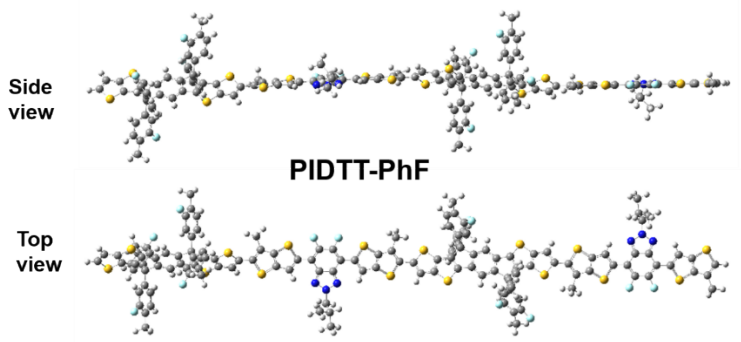

Figure S11. Density functional theory (B3LYP/6-31 G(*d*, *p*)) simulations of the three polymers.

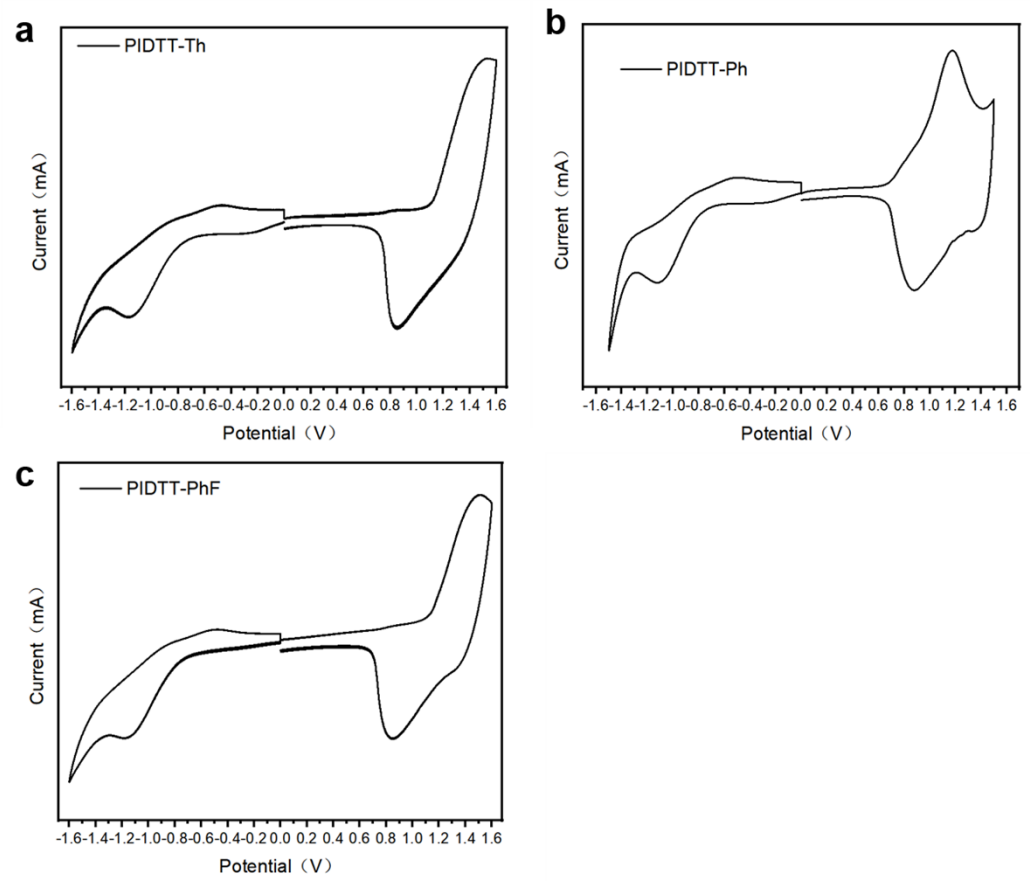

Figure S12. Cyclic voltammetry curves of (a) PIDTT-Th, (b) PIDTT-Ph, and (c) PIDTT-PhF.

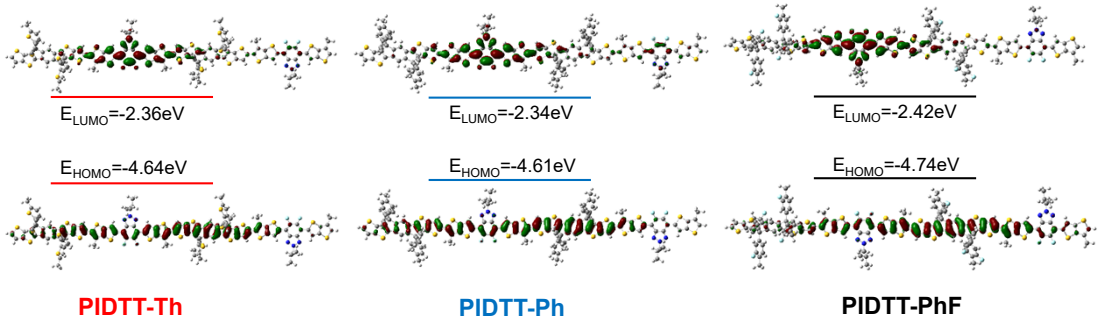

Figure S13. The electronic cloud distribution and optimized molecular orbitals of **PIDTT-Th**, **PIDTT-Ph** and **PIDTT-PhF** based on DFT simulation.

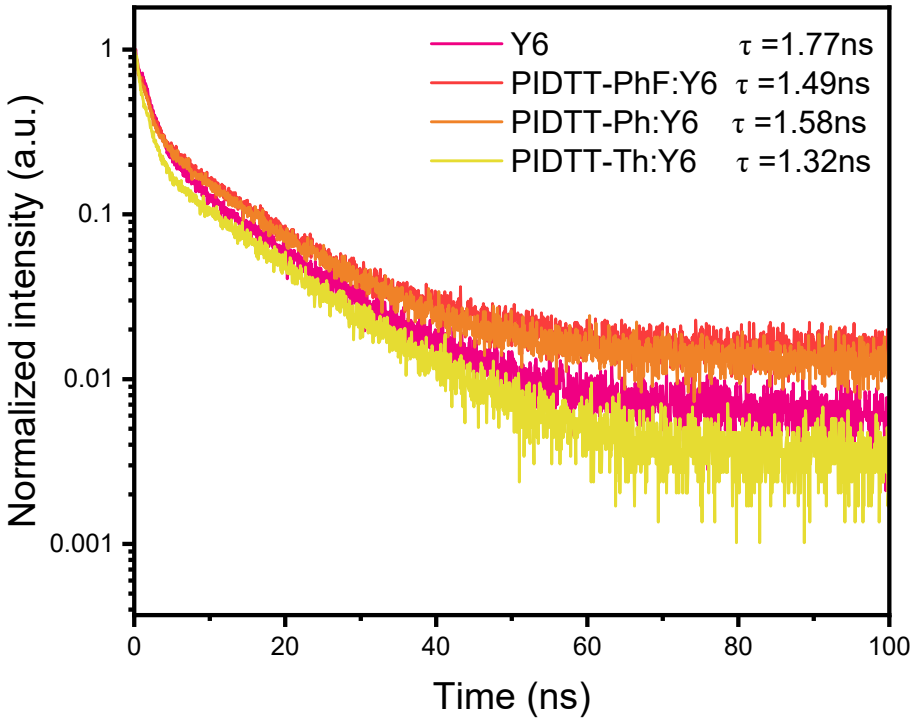

Figure S14. TRPL curves for Y6 neat film and **PIDTT-Th**:Y6, **PIDTT-Ph**:Y6 and **PIDTT-PhF**:Y6 blend films.

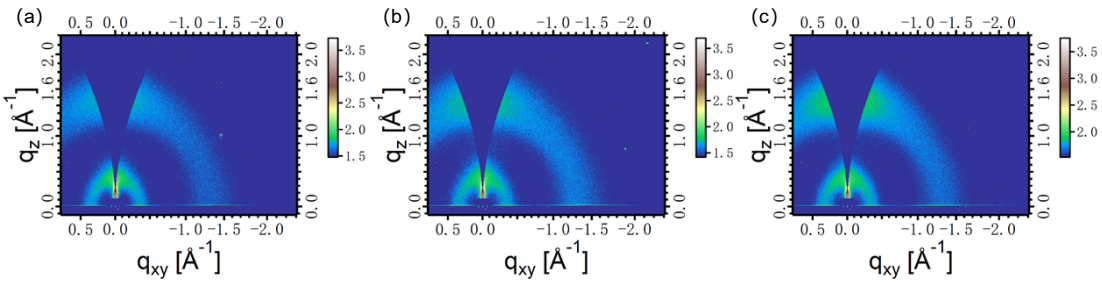

Figure S15. 2D GIWAXS patterns of pure copolymers (a) **PIDTT-Th**, (b) **PIDTT-Ph**, and (c) **PIDTT-PhF**.

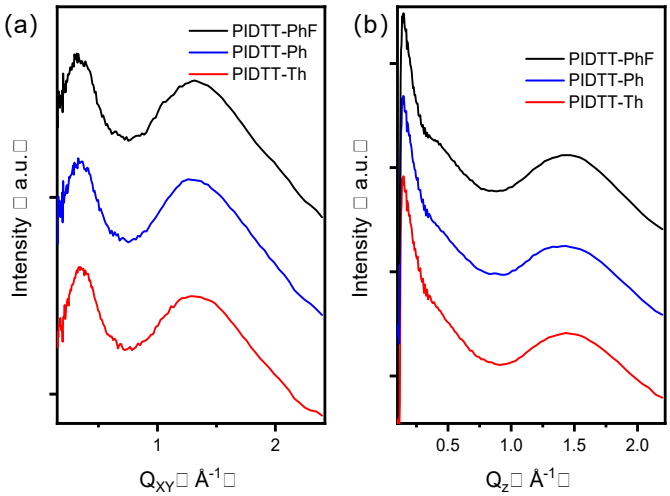

Figure S16. 1D profiles of pure films **PIDTT-Th**, **PIDTT-Ph**, and **PIDTT-PhF** (a) in-plane and (b) out-of-plane direction.

Table S1. Optical and electrochemical parameters of the three polymers and Y6.

Materials	λ_{max} (nm)		λ_{onset} (nm)	HOMO	LUMO	HOMO	LUMO	E_g^{opt}
	solution	film	film	(eV)[a]	(eV)[a]	(eV)[b]	(eV)[b]	(eV)[c]
PIDTT-PhF	517	525	605	-5.38	-3.65	-4.74	-2.42	2.05
PIDTT-Ph	511	511	610	-5.27	-3.59	-4.61	-2.34	2.03
PIDTT-Th	510	511	610	-5.25	-3.59	-4.64	-2.36	2.03
Y6	733	817	910	-5.65	-4.10	–	–	1.36

[a] LUMO and HOMO were calculated by CV curve; [b] LUMO and HOMO were calculated by DFT simulations; [c] The optical bandgaps were calculated by 1240/λ_{onset}.

Table S2. The photovoltaic performance of **Polymers**: Y6 under different solvent additives.

Device	Additive	V_{OC} (V)	J_{SC} (mA cm^{-2})	FF (%)	PCE (%)
PIDTT-Th: Y6	0.5%DIO	0.668	23.24	59.38	9.22
1:1.5	0.5%CN	0.713	21.09	56.4	8.48
15 mg mL^{-1} TA 150°C	0.5%DPE	0.697	23.59	56.26	9.25
PIDTT-Ph: Y6	0.5%DIO	0.695	24.64	60.84	10.42

1:1.5	0.5%CN	0.727	16.31	57.94	6.87
15 mg mL^{-1} TA 200℃	0.5%DPE	0.711	23.68	63.68	10.72
PIDTT-PhF: Y6	0.5%DIO	0.828	23.13	60.15	11.52
1:1.5	0.5%CN	0.86	14.46	48.32	6.01
15 mg mL^{-1} TA 150℃	0.5%OD	0.837	19.25	54.55	8.79

Table S3. The photovoltaic performance of **Polymers**: Y6 under different thermal annealing temperature.

Device	Annealing (℃)	V_{OC} (V)	J_{SC} (mA cm^{-2})	FF (%)	PCE (%)
PIDTT-Th: Y6	150	0.762	19.68	58.56	8.78
1:1.5	170	0.707	21.71	59.43	9.12
15 mg mL^{-1}	200	0.622	21.7	61.75	8.34
PIDTT-Ph: Y6	150	0.79	18.25	51.18	7.38
1:1.5	170	0.771	20.33	54.87	8.6
15 mg mL^{-1}	200	0.717	23.65	52.54	8.91
PIDTT-PhF: Y6	150	0.806	23.14	66.86	12.47
1:1.5	170	0.793	23.11	66.31	12.15
15 mg mL^{-1}	200	0.777	23.52	63.2	11.55

Table S4. The photovoltaic performance of **Polymers**: Y6 under different D: A ratios.

Device	D: A	V_{OC} (V)	J_{SC} (mA cm^{-2})	FF (%)	PCE (%)
PIDTT-Th: Y6	1.0:1.5	0.707	21.71	59.43	9.12
15 mg mL^{-1}	1.0:1.0	0.71	22.75	58.2	9.4
TA 170℃	1.5:1.0	0.71	22.53	58.2	9.31
PIDTT-Ph: Y6	1.0:1.5	0.771	20.33	54.87	8.6
15 mg mL^{-1}	1.0:1.0	0.787	16.07	46.03	5.82
TA 170℃	1.5:1.0	0.791	13.2	38.41	4.01

PIDTT-PhF: Y6	1.0:1.0	0.88	11.78	41.2	4.27
15 mg mL^{-1} TA 150℃	1.5:1.0	0.89	9.58	37.99	3.24

Table S5. Summary of device parameters of IDTT-based polymer as donor in OPVs.

Donor	Acceptor	V_{OC} (V)	J_{SC} (mA cm^{-2})	FF	PCE (%)	Ref.
PIDTT-DFBT	$PC_{71}BM$	0.95	12.21	0.61	7.03	2
PIDTTFBT	$PC_{71}BM$	0.90	10.08	0.46	4.20	3
PIDTTTPD	$PC_{71}BM$	0.90	7.99	0.60	4.30	3
PIDTT-TzTz	$PC_{71}BM$	0.90	10.41	0.59	5.53	4
PIDTT-TzTz	$PC_{71}BM$	0.90	10.99	0.59	5.90[a]	4
PIDTT-TzTz-TT	$PC_{71}BM$	0.89	9.51	0.52	4.40	4
PIDTT-Q-*p*	$PC_{71}BM$	0.83	7.20	0.63	3.70	5
PIDTT-Q-*m*	$PC_{71}BM$	0.81	11.80	0.70	6.70	5
PIDTT-QF-*p*	$PC_{71}BM$	0.92	6.70	0.60	3.70	5
PIDTT-QF-*m*	$PC_{71}BM$	0.95	5.70	0.63	3.30	5
PIDTTQ	$PC_{71}BM$	0.84	11.45	0.62	6.01	6
PIDTT-F-PhanQ-EH	$PC_{71}BM$	0.90	10.31	0.55	5.14	7
PIDTT-DFBT-EH	$PC_{71}BM$	0.95	11.16	0.52	5.48	7
PIDTT-DFBT-T	$PC_{71}BM$	0.91	9.50	0.50	4.40	8
PIDTT-DFBT-TT	$PC_{71}BM$	0.96	11.90	0.63	7.20	8
PIDTT-T-DFBT	$PC_{71}BM$	0.92	10.40	0.54	5.26	9
PIDTT-DTBTz	$PC_{71}BM$	0.84	9.73	0.62	5.07	10
PIDTT-BTz	$PC_{71}BM$	0.90	9.37	0.54	4.55	10
PIDTT-TT	$PC_{71}BM$	0.96	10.96	0.65	6.98	11
PIDTT-TID	$PC_{71}BM$	1.00	12.60	0.53	6.70	12
PhIDTT-Q	$PC_{71}BM$	0.81	9.69	0.58	4.30	13
PhIDTT-QF	$PC_{71}BM$	0.90	8.11	0.54	3.80	13
ThIDTT-Q	$PC_{71}BM$	0.87	10.50	0.58	5.30	13
ThIDTT-QF	$PC_{71}BM$	0.92	10.90	0.53	5.10	13
CTL1	$PC_{71}BM$	0.83	12.50	0.55	6.20	14
CTL2	$PC_{71}BM$	0.87	11.20	0.55	5.30	14
CTL3	$PC_{71}BM$	0.92	11.20	0.60	6.10	14
CTL4	$PC_{71}BM$	0.85	6.30	0.54	2.90	14
CTL5	$PC_{71}BM$	0.87	8.70	0.49	3.80	14
CTL6	$PC_{71}BM$	0.88	9.50	0.48	3.90	14
PIDTT-DFQ-T	$PC_{71}BM$	0.92	11.4	0.66	6.90	15
PIDTT-DFQ-Se	$PC_{71}BM$	0.89	12.3	0.65	7.10	15
PIDTT-DTBO	$PC_{71}BM$	0.88	10.50	0.49	4.47	16
PIDTT-DTBT	$PC_{71}BM$	0.86	10.20	0.56	4.79	16
PIDTT-DTBT	$PC_{61}BM$	0.81	5.51	0.46	2.05	17
PIDTT-TBT	$PC_{71}BM$	0.88	11.08	0.60	5.84	17

PIDTT-TFBT	$PC_{61}BM$	0.95	5.95	0.52	2.92	[17]
PIBTO-T	$PC_{71}BM$	0.87	12.09	0.62	6.52	[18]
PIBTO-TT	$PC_{71}BM$	0.88	13.06	0.65	7.52	[18]
2T-3MT	$PC_{71}BM$	0.92	7.35	0.48	3.28	[19]
PIDTT-Qx	$PC_{71}BM$	0.92	9.30	0.53	4.54	[20]
PIDTT-quinoxaline	$PC_{71}BM$	0.84	11.26	0.53	5.05	[21]
PIDTT-QxN2	$PC_{71}BM$	0.75	11.73	0.56	4.90	[22]
IDTT-QxCN	$PC_{71}BM$	0.89	12.26	0.51	5.47	[23]
2T-3MT	IM-IDT	1.01	6.81	0.58	3.96	[19]
2T-3MT	ITIC	0.99	4.78	0.35	1.67	[19]
PIDTTQ	$PC_{71}BM$	0.84	8.62	0.60	4.32	[24]
P1	$PC_{71}BM$	0.81	10.87	0.47	3.95	[24]
IDTT-T1	$PC_{71}BM$	0.92	11.25	0.62	6.58	[25]
XPL4	$PC_{71}BM$	0.94	11.11	0.54	5.85	[26]
XPL6	$PC_{71}BM$	0.95	9.50	0.55	5.13	[26]
PhIDTT-TQxT	$PC_{71}BM$	0.82	11.21	0.47	4.29	[27]
PIDTT-DTNT-C16	$PC_{71}BM$	0.83	4.67	0.34	1.30	[28]
PIDTT-DTNT-HD	$PC_{71}BM$	0.83	9.35	0.43	3.31	[28]
PIDTT-DTNT-OD	$PC_{71}BM$	0.80	3.70	0.34	1.02	[28]
PIDTT-Phz[a]	$PC_{71}BM$	0.86	13.60	0.58	6.70	[29]
PIDTT-Qx	$PC_{71}BM$	0.81	15.10	0.57	7.20	[29]
PIDTT-O	$PC_{71}BM$	0.85	8.64	0.55	4.06	[30]
PIDTT-S	$PC_{71}BM$	0.86	9.92	0.72	6.12	[30]
PIDTT-QxM	Y6BO	0.73	23.25	0.61	10.40	[31]
PIDTT-DTffBTA	Y6	0.74	22.70	0.66	11.05	[32]

[a] inverted device

Table S6. The detailed corresponding carrier mobility data of the three compounds

Blend	Electron mobility ($cm^2 V^{-1}s^{-1}$)	Thickness (nm)	Hole mobility ($cm^2 V^{-1}s^{-1}$)	Thickness (nm)
PIDTT-Th: Y6	1.9×10^{-4}	101.73	3.8×10^{-5}	100.26
PIDTT-Ph: Y6	3.4×10^{-4}	107.55	1.7×10^{-4}	104.3
PIDTT-PhF: Y6	2.3×10^{-4}	90.83	2.4×10^{-4}	119.35

Table S7. The detailed energy losses of OPVs based on PIDTT-Th: Y6, PIDTT-Ph: Y6 and PIDTT-PhF: Y6.

Blend	E_g (eV)	E_{CT} (eV)	V_{OC} (V)	ΔE (eV)	ΔE_1 (eV)	ΔE_2 (eV)	ΔE_3 (eV)	EQE_{EL} (%)
PIDTT-Th: Y6	1.386	1.35	0.71	0.676	0.036	0.300	0.340	2.01×10^{-4}
PIDTT-Ph: Y6	1.384	1.36	0.71	0.674	0.024	0.316	0.334	2.45×10^{-4}

PIDTT-PhF: Y6	1.384	1.37	0.81	0.574	0.014	0.318	0.242	8.87×10^{-3}

Table S8. The detailed parameters of GIWAXS measurement.

Films	In-plane		Out-of-plane			
	(100)	*d* (Å)	(010)	$d_{\pi\text{-}\pi}$ (Å)	FWHM (Å)	CL (Å)
PIDTT-Th	0.34	18.32	1.43	4.39	0.55	10.69
PIDTT-Ph	0.34	18.32	1.43	4.39	0.57	10.18
PIDTT-PhF	0.34	18.71	1.47	4.28	0.55	10.66
PIDTT-Th:Y6	0.28	22.60	1.75	3.59	0.35	16.60
PIDTT-Ph:Y6	0.27	23.02	1.75	3.59	0.32	18.09
PIDTT-PhF:Y6	0.27	23.02	1.75	3.59	0.37	15.83

References

(1) Wang, J. L.; Liu, K. K.; Yan, J.; Wu, Z.; Liu, F.; Xiao, F.; Chang, Z. F.; Wu, H. B.; Cao, Y.; Russell, T. P. Series of Multifluorine Substituted Oligomers for Organic Solar Cells with Efficiency over 9% and Fill Factor of 0.77 by Combination Thermal and Solvent Vapor Annealing. *J. Am. Chem. Soc.* **2016**, *138*, 7687-7697.

(2) Yun-Xiang Xu ; Chu-Chen Chueh ; Hin-Lap Yip ; Fei-Zhi Ding ; Yong-Xi Li ; Chang-Zhi Li ; Xiaosong Li ; Wen-Chang Chen ; Jen, A. K.-Y. Improved Charge Transport and Absorption Coefficient in Indacenodithieno[3,2-B]Thiophene-Based Ladder-Type Polymer Leading to Highly Efficient Polymer Solar Cells. *Adv. Mater.* **2012**, *24*, 6356–6361.

(3) Chang, H.-H.; Tsai, C.-E.; Lai, Y.-Y.; Chiou, D.-Y.; Hsu, S.-L.; Hsu, C.-S.; Cheng, Y.-J. Synthesis, Molecular and Photovoltaic Properties of Donor–Acceptor Conjugated Polymers Incorporating a New Heptacylic Indacenodithieno[3,2-B]Thiophene Arene. *Macromolecules* **2012**, *45*, 9282-9291.

(4) Xu, Y.-X.; Chueh, C.-C.; Yip, H.-L.; Chang, C.-Y.; Liang, P.-W.; Intemann, J. J.; Chen, W.-C.; Jen, A. K. Y. Indacenodithieno[3,2-B]Thiophene-Based Broad Bandgap Polymers for High Efficiency Polymer Solar Cells. *Polym. Chem.* **2013**, *4*, 5220.

(5) Xu, X.; Li, Z.; Bäcke, O.; Bini, K.; James, D. I.; Olsson, E.; Andersson, M. R.; Wang, E. Effects of Side Chain Isomerism on the Physical and Photovoltaic Properties of Indacenodithieno[3,2-B]Thiophene–Quinoxaline Copolymers: Toward a Side Chain Design for Enhanced Photovoltaic Performance. *J. Mater. Chem. A.* **2014**, *2*, 18988-18997.

(6) Gasparini, N.; Katsouras, A.; Prodromidis, M. I.; Avgeropoulos, A.; Baran, D.; Salvador, M.; Fladischer, S.; Spiecker, E.; Chochos, C. L.; Ameri, T.; et al. Photophysics of Molecular-Weight-Induced Losses in Indacenodithienothiophene-Based Solar Cells. *Adv. Funct. Mater.* **2015**, *25*, 4898-4907.

(7) Zang, Y.; Xu, Y.-X.; Chueh, C.-C.; Li, C.-Z.; Chen, H.-C.; Wei, K.-H.; Yu, J.-S.; Jen, A. K. Y. Photovoltaic Performance of Ladder-Type Indacenodithieno[3,2-B]Thiophene-Based Polymers with Alkoxyphenyl Side Chains. *RSC Advances* **2015**, *5*, 26680-26685.

(8) Intemann, J. J.; Yao, K.; Li, Y.-X.; Yip, H.-L.; Xu, Y.-X.; Liang, P.-W.; Chueh, C.-C.; Ding, F.-Z.; Yang, X.; Li, X.; et al. Highly Efficient Inverted Organic Solar Cells through Material and Interfacial Engineering of Indacenodithieno[3,2-B]Thiophene-Based Polymers and Devices. *Adv. Funct. Mater.* **2014**, *24*, 1465-1473.

(9) Li, Y.; Yao, K.; Yip, H.-L.; Ding, F.-Z.; Xu, Y.-X.; Li, X.; Chen, Y.; Jen, A. K. Y. Eleven-Membered Fused-Ring Low Band-Gap Polymer with Enhanced Charge Carrier Mobility and Photovoltaic Performance. *Adv. Funct. Mater.* **2014**, *24*, 3631-3638.

(10) Negash, A.; Genene, Z.; Eachambadi, R. T.; Verstappen, P.; Van den Brande, N.; Kesters, J.; D'Haen, J.; Wang, E.; Vandewal, K.; Maes, W.; et al. Ladder-Type High Gap Conjugated Polymers Based on Indacenodithieno[3,2-B]Thiophene and Bithiazole for Organic Photovoltaics. *Org. Electron.* **2019**, *74*, 211-217.

(11) Lee, W.; Jung, J. W. A Wide Band Gap Polymer Based on Indacenodithieno[3,2-B]Thiophene for High-Performance Bulk Heterojunction Polymer Solar Cells. *J. Mater. Chem. A.* **2017**, *5*, 712-719.

(12) Wang, C.; Xu, X.; Zhang, W.; Bergqvist, J.; Xia, Y.; Meng, X.; Bini, K.; Ma, W.; Yartsev, A.; Vandewal, K.; et al. Low Band Gap Polymer Solar Cells with Minimal Voltage Losses. *Adv. Energy Mater.* **2016**, *6*.

(13) Tatsi, E.; Spanos, M.; Katsouras, A.; Squeo, B. M.; Ibraikulov, O. A.; Zimmermann, N.; Heiser, T.; Lévêque, P.; Gregoriou, V. G.; Avgeropoulos, A.; et al. Effect of Aryl Substituents and Fluorine Addition on the Optoelectronic Properties and Organic Solar Cell Performance of a High Efficiency Indacenodithienothiophene-Alt-Quinoxaline π-Conjugated Polymer. *Macromol. Chem. Phys.* **2019**, *220*, 1800418.

(14) Chochos, C. L.; Leclerc, N.; Gasparini, N.; Zimmerman, N.; Tatsi, E.; Katsouras, A.; Moschovas, D.; Serpetzoglou, E.; Konidakis, I.; Fall, S.; et al. The Role of Chemical Structure in Indacenodithienothiophene-Alt-Benzothiadiazole Copolymers for High Performance Organic Solar Cells with Improved Photo-Stability through Minimization of Burn-in Loss. *J. Mater. Chem. A.* **2017**, *5*, 25064-25076.

(15) Wang, H. C.; Li, Q. Y.; Yin, H. B.; Ren, X.; Yao, K.; Zheng, Y.; Xu, Y. X. Synergistic Effects of Selenophene and Extended Ladder-Type Donor Units for Efficient Polymer Solar Cells. *Macromol. Rapid Commun.* **2018**, *39*, 1700483.

(16) Cai, P.; Xu, X.; Sun, J.; Chen, J.; Cao, Y. Effects of Including Electron-Withdrawing Atoms on the Physical and Photovoltaic Properties of Indacenodithieno[3,2-B]Thiophene-Based Donor–Acceptor Polymers: Towards an Acceptor Design for Efficient Polymer Solar Cells. *RSC Advances* **2017**, *7*, 20440-20450.

(17) An, L.; Tong, J.; Huang, Y.; Liang, Z.; Li, J.; Yang, C.; Wang, X. Elevated Photovoltaic Performance in Medium Bandgap Copolymers Composed of Indacenodi-Thieno[3,2-B]Thiophene and Benzothiadiazole Subunits by Modulating the Pi-Bridge. *Polymers (Basel)* **2020**, *12*.

(18) Ma, Y.; Chen, H.; Tang, Y.; Wang, J.-Y.; Ma, W.; Zheng, Q. Modulation of Bulk Heterojunction Morphology through Small π-Bridge Changes for Polymer Solar Cells with Enhanced Performance. *J. Mater. Chem. C.* **2018**, *6*, 5999-6007.

(19) Hoang, M. H.; Park, G. E.; Phan, D. L.; Ngo, T. T.; Nguyen, T. V.; Park, C. G.; Cho, M. J.; Choi, D. H. Synthesis of Conjugated Wide-Bandgap Copolymers Bearing Ladder-Type Donating Units and Their Application to Non-Fullerene Polymer Solar Cells. *Macromolecular Research* **2018**, *26*, 844-850.

(20) Handoko, S. L.; Jin, H. C.; Whang, D. R.; Putri, S. K.; Kim, J. H.; Chang, D. W. Synthesis of Quinoxaline-Based Polymers with Multiple Electron-Withdrawing Groups for Polymer Solar Cells. *J. Ind. Eng. Chem.* **2019**, *73*, 192-197.

(21) Xu, X.; Cai, P.; Lu, Y.; Choon, N. S.; Chen, J.; Ong, B. S.; Hu, X. Synthesis of a Novel Low-Bandgap Polymer Based on a Ladder-Type Heptacyclic Arene Consisting of Outer Thieno[3,2-B]Thiophene Units for Efficient Photovoltaic Application. *Macromol. Rapid Commun.* **2013**, *34*, 681-688.

(22) Wardani, R. P.; Jin, H. C.; Kim, J. H.; Chang, D. W. Synthesis of Quinoxaline-Based D-A Type Conjugated Polymers for Photovoltaic Applications. *Mol. Cryst. Lip. Cryst.* **2020**, *705*, 15-21.

(23) Handoko, S. L.; Jin, H. C.; Whang, D. R.; Kim, J. H.; Chang, D. W. Effect of Cyano Substituent on Photovoltaic Properties of Quinoxaline-Based Polymers. *J. Ind. Eng. Chem.* **2020**, *86*, 244-250.

(24) Gasparini, N.; García-Rodríguez, A.; Prosa, M.; Bayseç, Ş.; Palma-Cando, A.; Katsouras, A.; Avgeropoulos, A.; Pagona, G.; Gregoriou, V. G.; Chochos, C. L.; et al. Indacenodithienothiophene-Based Ternary Organic Solar Cells. *Frontiers in Energy Research* **2017**, *4*, 40.

(25) Cai, Y.; Zhang, X.; Xue, X.; Wei, D.; Huo, L.; Sun, Y. High-Performance Wide-Bandgap Copolymers Based on Indacenodithiophene and Indacenodithieno[3,2-B]Thiophene Units. *J. Mater. Chem. C.* **2017**, *5*, 7777-7783.

(26) Chochos, C. L.; Katsouras, A.; Gasparini, N.; Koulogiannis, C.; Ameri, T.; Brabec, C. J.; Avgeropoulos, A. Rational Design of High-Performance Wide-Bandgap (Approximately 2 Ev) Polymer Semiconductors as Electron Donors in Organic Photovoltaics Exhibiting High Open Circuit Voltages (Approximately 1 V). *Macromol. Rapid Commun.* **2017**, *38*, 1600614.

(27) Chochos, C. L.; Singh, R.; Gregoriou, V. G.; Kim, M.; Katsouras, A.; Serpetzoglou, E.; Konidakis, I.; Stratakis, E.; Cho, K.; Avgeropoulos, A. Enhancement of the Power-Conversion Efficiency of Organic Solar Cells Via Unveiling an Appropriate Rational Design Strategy in Indacenodithiophene- Alt-Quinoxaline Pi-Conjugated Polymers. *ACS Appl. Mater.Interfaces* **2018**, *10*, 10236-10245.

(28) An, L.; Tong, J.; Yang, C.; Zhao, X.; Wang, X.; Xia, Y. Impact of Alkyl Side Chain on the Photostability and Optoelectronic Properties of Indacenodithieno[3,2‐B]Thiophene‐Alt‐Naphtho[1,2‐C:5,6‐C′]Bis[1,2,5]Thiadiazole Medium Bandgap Copolymers. *Polym. Int.* **2019**, *69*, 192-205.

(29) Kim, D. H.; Han, Y. W.; Moon, D. K. A Comparative Investigation of Dibenzo[a,C]Phenazine and Quinoxaline Donor–Acceptor Conjugated Polymers: Correlation of Planar Structure and Intramolecular Charge Transfer Properties. *Polymer* **2019**, *185*, 121906.

(30) Liu, S.; Yi, S.; Qing, P.; Li, W.; Gu, B.; He, Z.; Zhang, B. Molecular Engineering Enhances the Charge Carriers Transport in Wide Band-Gap Polymer Donors Based Polymer Solar Cells. *Molecules* **2020**, *25*, 4101.

(31) Wardani, R. P.; Jeong, M.; Lee, S. W.; Whang, D. R.; Kim, J. H.; Chang, D. W. Simple Methoxy-Substituted Quinoxaline-Based D-A Type Polymers for Nonfullerene Polymer Solar Cells. *Dyes Pigm.* **2021**, *192*, 109346.

(32) Li, F.; Tang, A.; Zhang, B.; Zhou, E. Indacenodithieno[3,2-B]Thiophene-Based Wide Bandgap D-pi-A Copolymer for Nonfullerene Organic Solar Cells. *ACS Macro Lett.* **2019**, *8*, 1599-1604.